Available online at www.sciencedirect.com
SCIENCE DIRECT
International Journal of Mass Spectrometry 253 (2006) 225–237
International Journal of Mass Spectrometry
www.elsevier.com/locate/ijms

G-quadruplexes in telomeric repeats are conserved in a solvent-free environment

Erin Shammel Baker [a], Summer L. Bernstein [a], Valérie Gabelica [b], Edwin De Pauw [b], Michael T. Bowers [a,*]

[a] *Department of Chemistry & Biochemistry, University of California, Santa Barbara, CA 93106, USA*
[b] *Laboratoire de Spectrométrie de Masse, Institut de Chimie (Bat. B6c), Université de Liège, B-4000 Liège, Belgium*

Received 19 March 2006; accepted 27 March 2006

Abstract

The structural properties of G-quadruplex forming sequences, such as the human telomeric repeat $d(T_2AG_3)_n$, are of great interest due to their role in cancer and cellular aging. To determine if G-quadruplexes are present in a solvent-free environment, different lengths of the telomeric repeat $d(T_2AG_3)_n$ (where $n = 1$, 2, 4 and 6) and dTG_4T were investigated with mass spectrometry, ion mobility and molecular dynamics calculations. Nano-ESI-MS illustrated quadruplex stoichiometries compatible with G-quadruplex structures for each sequence, with dT_2AG_3 and dTG_4T forming 4-strand complexes with two and three NH_4^+ adducts, $d(T_2AG_3)_2$ a 2-strand complex, and $d(T_2AG_3)_4$ and $d(T_2AG_3)_6$ remaining single-stranded. Experimental cross sections were obtained for all species using ion mobility methods. In all cases, these could be quantitatively matched to model cross sections with specific strand orientations (parallel/antiparallel) and structures. For each species, the solvent-free structures agreed with the solution CD measurements, but the ion mobility/modeling procedure often gave much more detailed structural information.

Keywords: Ion mobility; G-quadruplexes; DNA

1. Introduction

The survival of all living organisms depends on the stability of genomic information. In the late 1930s, Muller and McClintock revealed that one of the key elements for genomic stability is the end of chromosomes, called telomeres [1–5]. Telomeres consist of non-coding repetitive DNA sequences associated with proteins [6,7], and in all eukaryotic cells the telomeric DNA is double-stranded for most of its length and consists of a short tandem repeat sequence that is G-rich for the 3′ end and C-rich in the complementary strand. The tandem repeat is clearly related in many species as the G-rich strand contains repeats of the sequence $d(T_4G_4)_n$ for the protozoan *Oxytricha* [8], $d(T_2G_4)_n$ for the protozoan *Tetrahymena* [9] and $d(T_2AG_3)_n$ for all vertebrates [10–12]. An interesting characteristic of the telomere is that the extreme 3′ end of the G-rich strand is a single-stranded overhang and its integrity is essential for cell survival [10–12]. Single-stranded DNA regions are normally repaired by damage recognition systems, since they technically constitute a double-stranded break. However, telomeres are not recognized by DNA damage recognition systems and are stable structures not prone to degradation, recombination or fusions with other chromosome ends [13,14]. Thus, the survival of the single-stranded 3′ telomeric end is of great interest.

To study the 3′ overhang in telomeres, numerous structural investigations have been performed on single-strands with various telomere repeats sequences. These studies have revealed that these G-rich sequences are able to form G-quadruplex structures, which are made up of G-quartet subunits with four coplanar guanines (G) linked together by Hoogsteen hydrogen bonds (Scheme 1). Within each quadruplex, the G-quartets stack and are stabilized by coordination of the carbonyl oxygens in the guanines to specific monovalent (Na^+, K^+ or NH_4^+) or divalent cations (Sr^{2+}) as shown in Scheme 1 [15,16].

A variety of different G-quadruplex structures have been identified in vitro depending on strand stoichiometry, relative strand orientation and loop arrangement, which is a consequence of the former two. The adopted stoichiometry of the

* Corresponding author. Tel.: +1 805 893 2893; fax: +1 805 893 8703.
E-mail address: bowers@chem.ucsb.edu (M.T. Bowers).

1387-3806/$ – see front matter © 2006 Elsevier B.V. All rights reserved.
doi:10.1016/j.ijms.2006.03.016

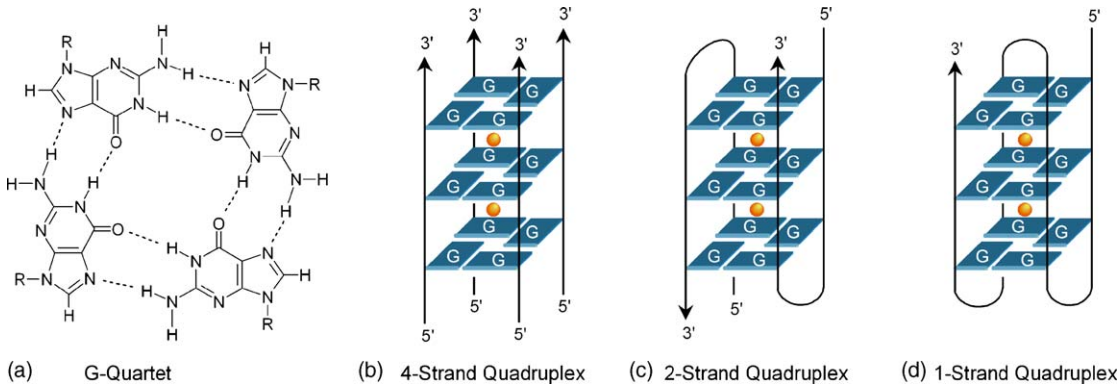

Scheme 1. (a) The structure of a G-quartet. The different strand arrangements for a (b) 4-strand intermolecular, (c) 2-strand intermolecular and (d) 1-strand intramolecular quadruplex. Metal cations are shown in orange.

G-quadruplex depends on how many G-rich repeats occur consecutively. If a DNA sequence has only one G-rich repeat, four strands can aggregate to form a 4-strand intermolecular quadruplex (Scheme 1b) [17,18]. If two G-rich repeats are present, a 2-strand intermolecular quadruplex is possible (Scheme 1c) [19,20], and sequences with four or more G-rich repeats can fold up on themselves to form 1-strand intramolecular quadruplexes [21,22]. Understanding these different quadruplex strand arrangements is essential because although there is ample evidence that quadruplexes form in vitro, currently no direct evidence of in vivo quadruplex structures exists. However, indirect support for the existence and role of quadruplexes in vivo is abundant as proteins that bind to quadruplexes [23,24], quadruplex specific nucleases [25] and some helicases that unwind quadruplexes have all been identified [26,27].

Multiple strand orientations are possible for each 1-, 2- and 4-strand quadruplex as shown in Scheme 2 [28,29]. Most studies have indicated that 4-strand quadruplexes normally have parallel strand orientations [17,18], while more complexity has been illustrated in the 1- and 2-strand human telomere quadruplexes. In the 2-strand quadruplex for $(dTAG_3T_2AG_3T)_2$, NMR indicated both parallel and antiparallel conformations exist in solution [30]. Regarding the 1-strand quadruplex for $dAG_3(T_2AG_3)_3$, there is still a debate on the structure adopted in solution. The NMR structure in the presence of Na^+ was an antiparallel basket quadruplex [31], but the X-ray structure for the same sequence in the presence of K^+ revealed a parallel propeller quadruplex [32]. A recent paper indicated that molecular crowding resulting from the crystallization conditions was the cause of the conversion in the K^+ solution structure to a propeller parallel structure [29], but another study based on circular dichroism favors a mixed parallel/antiparallel structure in the presence of K^+ [33]. All of these studies and structural variations indicate that further methods for analyzing quadruplex structures are needed.

Upon the discovery that quadruplexes form in the presence of NH_4^+ [34–38], a door was opened for quadruplex studies with mass spectrometry. Recently, ESI-MS studies have illustrated that stoichiometries suggestive of G-quadruplexes have been sprayed from solution and persist in the solvent-free environment of the mass spectrometer [39–45]. Rosu et al. studied the 4-strand $(dTG_4T)_4$, the 2-strand $(dG_4T_4G_4)_2$ and the single-strand quadruplex $dG_3(T_2AG_3)_3$ [43]. The detection of three ammonium adducts in the first two sequences was interpreted as an indirect proof that the guanine quartets were preserved, as $n-1$ cations insert between n quartets. Unfortunately, no ammonium adducts were detected with the telomeric repeat $dG_3(T_2AG_3)_3$,

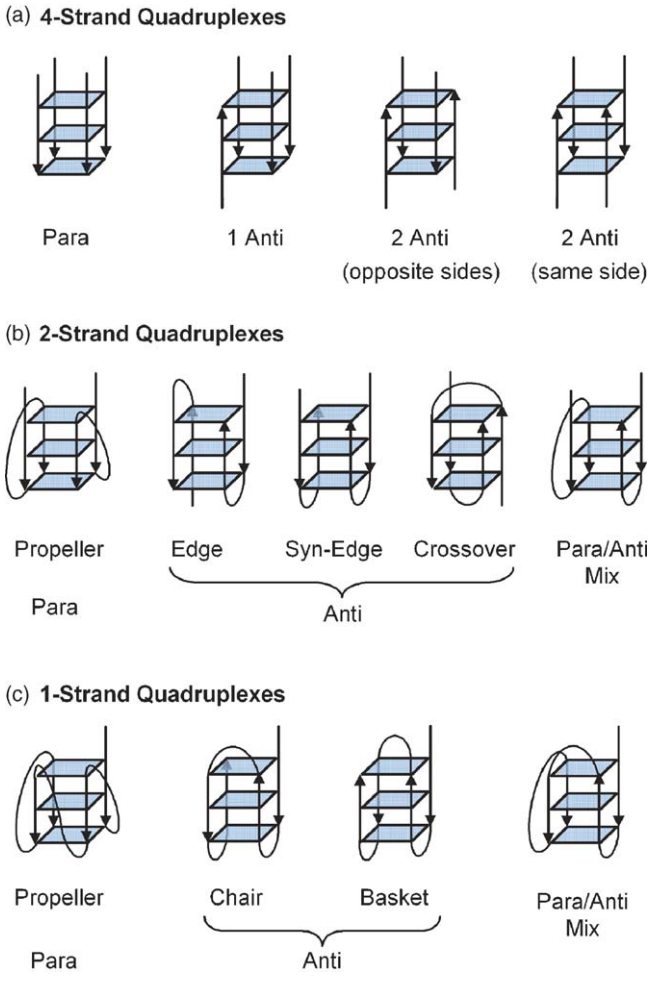

Scheme 2. Different strand orientations for (a) 4-strand intermolecular quadruplexes, (b) 2-strand intermolecular quadruplexes and (c) 1-strand intramolecular quadruplexes. Anti, antiparallel strand orientation and para, parallel.

so they could not prove that intramolecular quadruplexes formed by the telomeric sequence actually keep a folded G-quadruplex structures in a solvent-free environment. By using ion mobility [46–49] in conjunction with molecular mechanics/dynamics calculations, it has been observed that quadruplex structures formed in solution persist after evaporation of solvent for deoxyguanosine (dG) [44]. However, dG does not have a phosphate backbone, so it is essential to study longer DNA sequences to understand how the backbone and bases effect the quadruplex structure. In the present study dTG_4T and four different lengths of the human telomere sequence $d(T_2AG_3)_n$ (where $n = 1$, 2, 4 and 6) were analyzed with mass spectrometry, ion mobility and molecular dynamics calculations. For the sake of this paper, T1 = dT_2AG_3, T2 = $d(T_2AG_3)_2$, T4 = $d(T_2AG_3)_4$ and T6 = $d(T_2AG_3)_6$. Our goal in studying these sequences was to utilize ion mobility methods and molecular dynamics simulations to determine if these solvent-free quadruplex-compatible stoichiometries, with and without ammonium adducts, are actually quadruplex structures with well-conserved guanine quartets or just globular conformations.

2. Experimental method

2.1. Materials and sample preparation

dTG_4T, T1, T2, T4 and T6 were purchased from Integrated DNA Technologies, Inc. (Coralville, IA) and used without further purification. All samples were resuspended to a concentration of 300 μM in a 150 mM NH_4OAc/H_2O solution at pH 7. The samples were then annealed at 95 °C for 10 min, slowly cooled to room temperature and stored at 10 °C. Before use with nano-ESI, the solution was diluted to a final concentration of 100 μM with H_2O. Lower concentrations of DNA were also analyzed, but they gave results similar to the 100 μM samples.

2.2. Circular dichroism experiments

CD spectra were measured for the 100 μM DNA solutions on an AVIV 202 Circular Dichroism Spectrometer using a 0.1 cm path length quartz cell. For the CD experiments, the ellipticity of the 100 μM DNA solutions was monitored from 220 to 320 nm to determine the wavelengths where maximum and minimum ellipticity occurs.

2.3. Mass spectrometry and ion mobility experiments

The instrument used for the ion mobility measurements has previously been described in detail [50], so only a brief description is given here. Ions are generated by nano-ESI and injected into an ion funnel through a 3 inch. long capillary. The ion funnel essentially acts as an ion guide, compressing the stream of ions exiting the capillary and directing them toward the drift cell. The funnel is also used as an ion trap, allowing conversion of the continuous ion beam from the ESI source into a short ion pulse for the mobility measurements. After the ions are injected into a 4.5 cm long drift cell, they are quickly thermalized by collisions with ~5 Torr of helium gas and drift through the cell under the influence of a weak, uniform electric field (10–23 V/cm). Collisions with the helium buffer gas broaden the ion packet and serve to bring a balance between the force imposed by the electric field and the frictional drag force. As a consequence, the ions drift at constant velocity, v_d, proportional to the applied field E;

$$v_d = KE \tag{1}$$

The proportionality constant, K, is termed the mobility. In order to obtain values independent of temperature T and pressure p, the reduced mobility K_o is usually determined:

$$K_o = \left(K \cdot \frac{p}{760} \cdot \frac{273.16}{T} \right) \tag{2}$$

Once K_o is determined, kinetic theory is applied to express K_o as a function of the collision system parameters [51]:

$$K_o = \frac{3q}{16N} \left(\frac{2\pi}{\mu k_b T} \right)^{1/2} \frac{1}{\sigma} \tag{3}$$

where q is the ion charge, N the buffer gas density, μ the reduced mass of the collision partners, k_b the Boltzmann's constant and σ is the collision cross section.

As the ions exit the cell, they are mass analyzed with a quadrupole mass filter and detected as a function of time, yielding an arrival time distribution (ATD). Using Eqs. (1)–(3), it is straightforward to obtain an expression for the arrival time, t_A, in terms of the instrumental and molecular parameters:

$$t_A = \frac{l^2}{K_o} \cdot \frac{273.16}{760T} \cdot \frac{p}{V} + t_o \tag{4}$$

where l is the drift cell length, V the voltage across the cell and t_o is the time the ions spend outside the drift cell before detection. Hence, a plot of t_A versus p/V yields K_o from the slope and thus the cross section using Eq. (3). In a typical experiment, the pressure is held constant, while four or five different drift voltages are applied. The resultant plots are always linear with R^2 values greater than 0.9999.

In all experiments reported, the ATDs were measured over a wide range of injection voltages (30–100 eV). At low injection energies, the ions are gently pulsed into the cell and only need a few "cooling" collisions to reach thermal equilibrium with the buffer gas. However, at high injection energies, the larger collision energy leads to internal excitation of the ions before cooling and equilibrium occurs.

2.4. Theoretical calculations for model structures

Conformational analysis of the ions is obtained by comparing the experimental cross sections from ATDs to the cross sections of theoretical structures. Starting structures for dTG_4T, T1, T2, T4 and T6 were created using the antiparallel NMR structure 143D [31] and the mixed parallel and antiparallel NMR structure 186D [9,52]. The parallel structure for dTG_4T was created from 244D [53], while the parallel structures for T1, T2, T4 and T6 were created from 1KF1 [32]. HyperChem [54] was used to make alterations to the NMR and X-ray structures so that they matched the sequences being analyzed. 300 K molecular

dynamics simulations were run on each structure for 2 ns using the AMBER 7 set of programs [55] and every 5 ps a structure was saved. Each structure was then energy minimized and its cross section calculated using hard-sphere scattering and trajectory models developed by the Jarrold group [56,57]. In these calculations, each starting structure eventually converges to give at least one steady state structure where the cross section remains relatively constant. The average cross section of the final 50–100 structures in each steady state is then used for comparison with the experimental values.

The overall charge state of the quadruplexes can be readily identified from the mass spectra, but the exact locations of the deprotonation sites needed for the modeling are not known. Consequently, the same quadruplex structures were modeled with many different deprotonation sites, but no theoretical differences in cross section or conformation were observed as a function of charge location, in agreement with modeling results on duplex DNA published by Rueda et al. [58]. To model the same total charge for quadruplexes with and without NH_4^+, one phosphate group is deprotonated for each additional NH_4^+ inserted between the quartets.

An annealing/energy minimization cycle was used to generate globular structures for each sequence. In this cycle, an initial minimization of the structure is followed by 30 ps of molecular dynamics at 600 K and 10 ps of molecular dynamics in which the temperature is incrementally dropped to 50 K. The resulting structure is then energy minimized again and used as the starting structure for the next minimization/dynamics run. After all low-energy structures are obtained, the theoretical cross sections are calculated for comparison with experimental cross sections. A scatter plot of cross section versus energy is collected for the minimized structures and the average cross section of the lowest 5–10 kcal/mol structures are then compared to the experiment.

3. Results and discussion

3.1. Circular dichroism

Circular dichroism (CD) was utilized to characterize the solution conformations of the quadruplex sequences in an ammonium acetate solution, prior to electrospray. In the literature, quadruplex CD spectra have been reported previously in Na^+ and K^+, but not in NH_4^+. CD is a very valuable tool because it allows assignment of the quadruplex strand orientations in solution as either parallel or antiparallel (Scheme 2). Parallel quadruplexes have a maximum ellipticity near 265 nm and a minimum near 240 nm, while antiparallel quadruplexes have a maximum near 295 nm and a minimum near 260 nm [38,59]. Fig. 1 illustrates the CD spectra for the five different sequences analyzed. dTG_4T and T1 both illustrate parallel quadruplex properties. The CD spectrum for T2 has maxima at 265 and 295 nm, which are characteristic of both parallel and antiparallel folding. NMR studies have also revealed the presence of parallel and antiparallel conformations for sequences similar to T2 in K^+ solutions, so the CD spectrum for T2 in ammonium acetate seems to be consistent with other solution data [30]. The CD spectra of T4 and T6 in ammonium acetate show a strong maximum at 295 nm, a shoulder at 270 nm, another maximum around 245 nm, and two small minima around 260 and 235 nm. The major species corresponds to an antiparallel quadruplex like that formed in NaCl solution [28,33]. However, there could be a contribution of a minor species with structural properties like the Tetrahymena quadruplex which has both parallel and antiparallel loops (model structure at the bottom left of Scheme 2), and gives a CD spectrum with a maximum at 265 nm [33]. However the relative intensity of this shoulder is lower than in a K^+ solution, so the major species in ammonium acetate is most likely an antiparallel quadruplex.

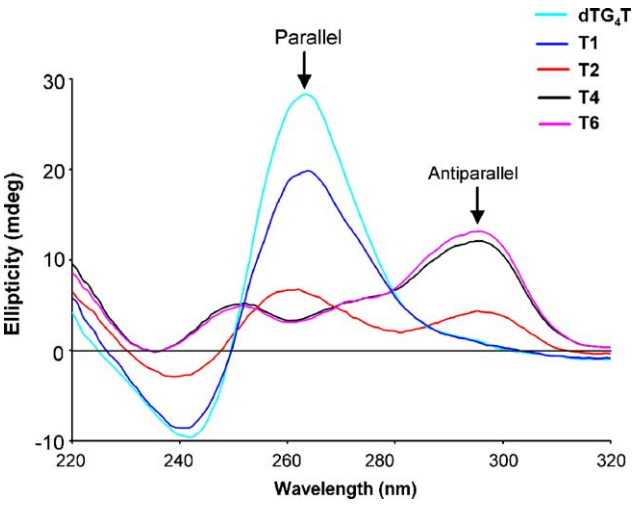

Fig. 1. CD spectra for dTG_4T, T1, T2, T4 and T6. dTG_4T and T1 exhibit a maximum at ~265 nm which is characteristic of parallel folds, T4 and T6 have a maximum at ~295 nm characteristic of antiparallel folding, and T2 has maxima at both 265 and 295 nm indicating that both antiparallel and parallel folds exist. Positions of maximum ellipticity for parallel and antiparallel folds are indicated by arrows.

3.2. Mass spectra

The nano-ESI mass spectra for dTG_4T, T1, T2, T4 and T6 are shown in Fig. 2. The mass spectra for dTG_4T and T1 both indicate the presence of a 4-strand complex with −5 and −6 charge states (Fig. 2a and b). However, differences are observed in the number of NH_4^+ adducts that are attached to the 4-strand complexes. The dominant peak for the 4-strand T1 complex has two NH_4^+ adducts, while the dominant peak for the 4-strand dTG_4T complexes has three NH_4^+ adducts. Since metal cations are known to sit between each G-quartet layer to stabilize a quadruplex, if these species are indeed quadruplexes then it is reasonable that the three quartet layers in T1 would posses $2NH_4^+$, while the four quartet layers for dTG_4T would have three NH_4^+ ions. It should be noted however, that the dominant ESI-MS peaks for DNA duplexes sprayed from ammonium acetate solutions do not have NH_4^+ adducts [60], consequently, the ammonium ions in the 4-strand complexes must be bound very tightly.

The mass spectrum for T2 indicates the presence of a $(T2)_2^{5-}$ complex (Fig. 2c). A 2-strand complex in a −6 charge state may

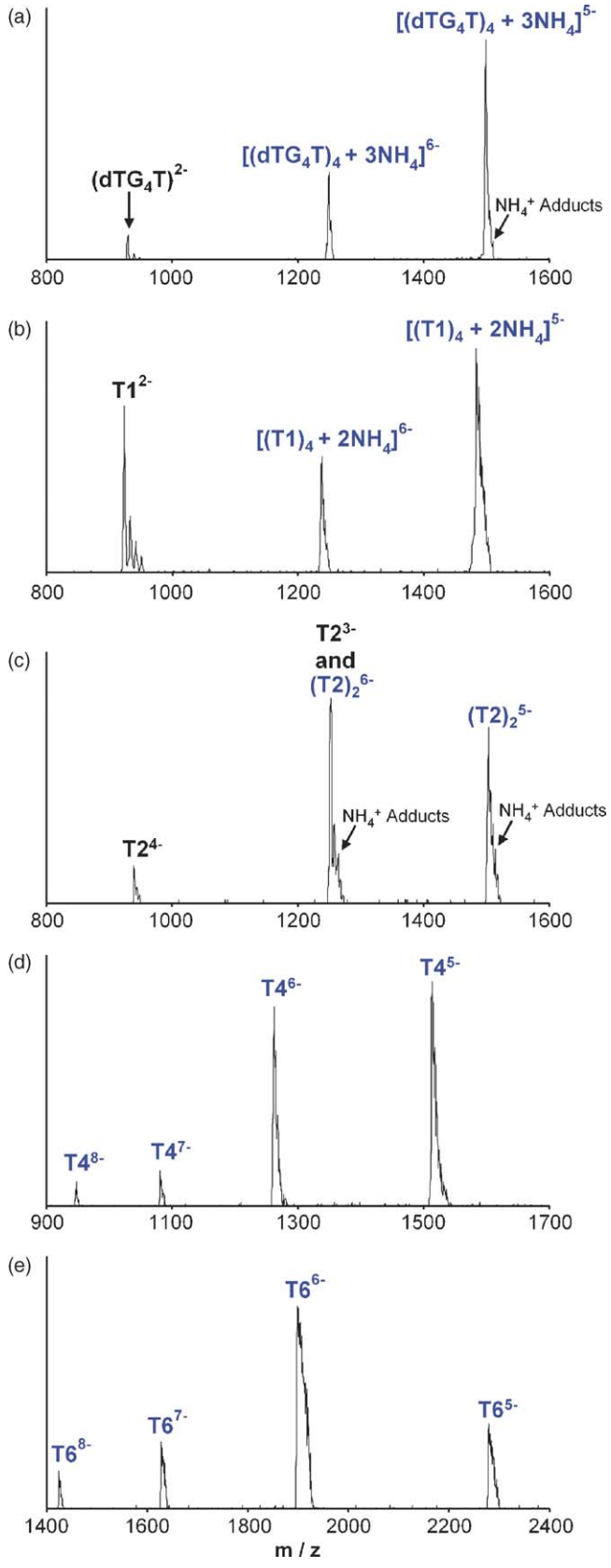

Fig. 2. Nano-ESI mass spectra for (a) dTG_4T, (b) T1, (c) T2, (d) T4 and (e) T6. The dominant peaks for the 4-strand complexes of T1 and dTG_4T have 2 and 3 NH_4^+ adducts, while the dominant peaks for $(T2)_2$, T4 and T6 do not have NH_4^+ adducts. All possible quadruplex stoichiometries are shown in blue. The background was subtracted on the spectra to clearly illustrate the peaks.

also be present, but due to its overlap with the −3 charge state of the T2 single-strand it could not be definitively assigned from the mass spectrum alone. The 2-strand T2 complex cannot be a Watson–Crick duplex since the strands are not complementary, suggesting this complex may correspond to a 2-strand quadruplex with no ammonium cations inside. In the mass spectra for T4 and T6, single-strands of multiple charge states exist, which could correlate to intramolecular 1-strand quadruplexes (Fig. 2d and e). One interesting observation is that the dominant mass spectral peaks for the 2-strand complex of T2 and the single-strands of T4 and T6 do not have NH_4^+ adducts like the 4-strand T1 and dTG_4T complexes. NH_4^+ adducts are present to the right of each peak, but they are not the dominant species in the mass spectra. Rosu et al. observed similar trends in their ESI-MS analysis of dTG_4T, $d(G_4T_4G_4)_2$ and $dG_3(T_2AG_3)_4$, which they attributed to the conformation strain induced by the loops of the quadruplex [43]. Unfortunately, using mass spectra alone, they could not prove whether quadruplexes structures actually exist in the solvent-free environment of their instrument. Here, we will use ion mobility measurements and molecular dynamics modeling to determine whether quadruplex structures are present.

3.3. Ion mobility

In order to determine if the solution phase quadruplex structures for dTG_4T, T1, T2, T4 and T6 survive the nano-ESI process, ion mobility experiments were performed. For all systems, the ions were gently injected from the ion funnel into the drift cell in order to minimize structural rearrangement or dissociation of oligomers.

3.3.1. 4-Strand quadruplexes: dTG_4T and T1

A typical ATD obtained for the −5 and −6 charge states of $[(dTG_4T)_4 + 3NH_4]$ and $[(T1)_4 + 2NH_4]$ is shown in Fig. 3. Only one peak occurs in each ATD, and a single symmetric peak indicates that most likely only one family of conformers is present. Experimental cross sections were extracted from the ATDs for each −5 complex and are listed in Table 1. Values for the −6 complexes were also measured, but they were within 1% of the −5 cross sections, so they are not included in the table.

In order to assign structures to the cross sections determined from the ATDs, 300 K molecular dynamics calculations were performed. Four different strand orientations are possible for a 4-strand quadruplex where the strands can either be all parallel, three parallel with one antiparallel, two parallel with two antiparallel next to each other, or two parallel with two antiparallel across from each other (Scheme 2). Each of these strand orientations were used as starting structures for 300 K molecular dynamics. Only one steady state structural family was observed during the dynamics for each of the different quadruplexes. The cross sections for the −5 quadruplexes are listed in Table 1 and similar cross sections were obtained for the −6 quadruplexes.

Theoretical structures obtained from 300 K dynamics simulations for the parallel strand orientation of $[(dTG_4T)_4 + 3NH_4]^{5-}$

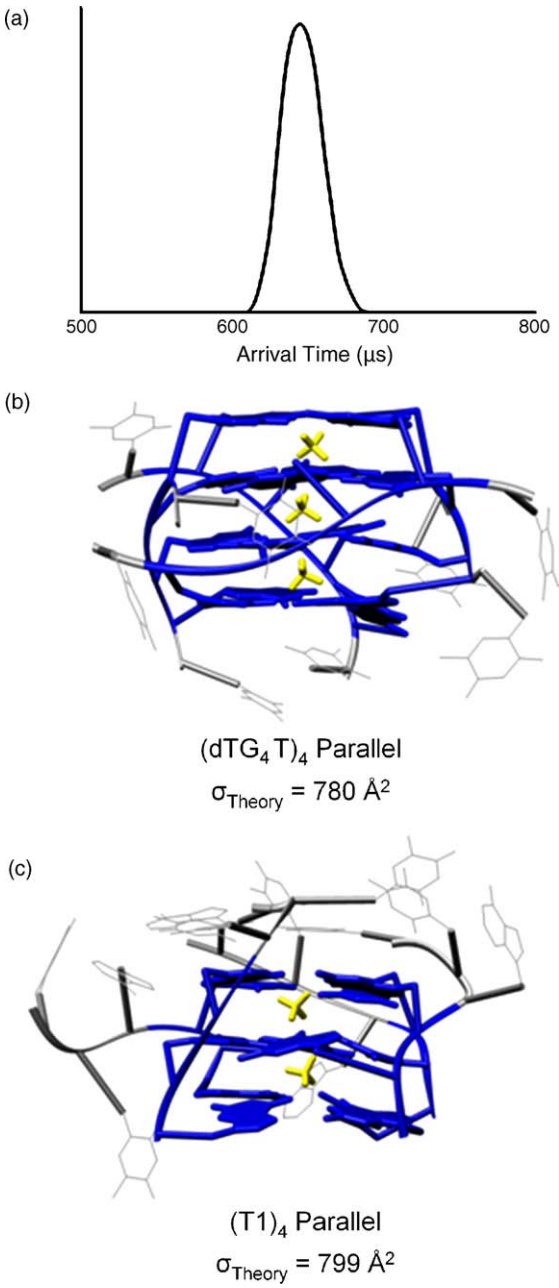

Fig. 3. (a) A single peak ATD was acquired for the −5 and −6 charge states of $[(dTG_4T)_4 + 3NH_4]$ and $[(T1)_4 + 2NH_4]$. The ATD shown is for $[(dTG_4T)_4 + 3NH_4]^{5-}$ with a cross section of 775 Å^2. Parallel quadruplex structures for (b) $[(dTG_4T)_4 + 3NH_4]^{5-}$ and (c) $[(T1)_4 + 3NH_4]^{5-}$ that match the experimental cross sections.

and $[(T1)_4 + 2NH_4]^{5-}$ are shown in Fig. 3. In all of the different strand orientations for the 4-strand quadruplexes, all of the Hoogsteen bonds remained intact and the NH_4^+ ions sit between the quartets. $[(dTG_4T)_4 + 3NH_4]$ was assigned to a quadruplex conformation as the globular conformation is too small. However, from ion mobility and molecular dynamics, distinction between the parallel and antiparallel quadruplexes could not be made due to size similarities, since no matter whether a dTG_4T strand is parallel or antiparallel, one thymine is above the quadruplex and one thymine is below. On the other hand, the only structure that agreed with the experimental cross section for $[(T1)_4 + 2NH_4]^{5-}$ was the parallel quadruplex since the globular cross section was too small and the antiparallel arrangements were too large (Table 1). Recall that CD experiments indicate that T1 and dTG_4T have parallel strand orientations in solution (Fig. 1). Since the parallel orientation of T1 is retained after spraying, it is probable that dTG_4T also

Table 1
Experimental and theoretical cross sections (Å^2) for $[(dTG_4T)_4 + 3NH_4]^{5-}$ and $[(T1)_4 + 2NH_4]^{5-}$ [a]

Complex[b]	Cross sections[c]	
	$[(dTG_4T)_4 + 3NH_4]^{5-}$	$[(T1)_4 + 2NH_4]^{5-}$
Experimental	775	805
Theoretical		
Globular	740	740
4 Para	780[d]	799[e]
1 Anti	782[d]	830
2 Anti opposite	778[d]	824
2 Anti together	779[d]	825

[a] Cross sections for the −6 charge state were within 1%.
[b] Para, parallel and Anti, antiparallel.
[c] 1% reproducibility error for the experimental cross sections and ≤2% S.D. for the theoretical values.
[d] Both parallel and antiparallel strand orientations agree with the experimental cross section for $[(dTG_4T)_4 + 3NH_4]^{5-}$.
[e] Only a parallel strand orientation agrees for $[(T1)_4 + 2NH_4]^{5-}$.

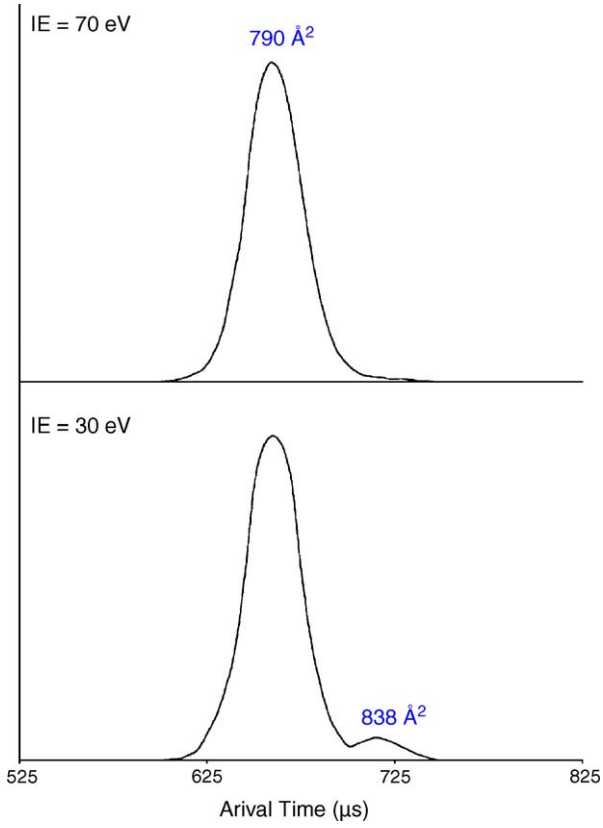

Fig. 4. Two peaks were observed in the ATDs for $(T2)_2^{5-}$ and $[(T2)_2 + 2NH_4]^{5-}$ at low injection energies (30 eV). However, as the injection energy was raised, the small peak at 715 μs diminishes.

retains its parallel conformation and no structural rearrangement occurs.

3.3.2. 2-Strand quadruplex: T2

The ATDs for $(T2)_2^{5-}$ are shown in Fig. 4. Both of the ATDs were obtained under similar experimental conditions except injection energy, which was set at a low and high voltage. At the lowest injection energy two peaks are present, signifying that two different conformers exist in a 9:1 ratio. However, at the higher injection energy, the weaker longer time peak, corresponding to the more extended conformer, diminishes to be almost unobservable. The cross section of each peak was measured yielding 790 Å^2 for the shorter time peak and 838 Å^2 for the longer time peak. To understand the effect of NH_4^+ stabilization on $(T2)_2^{5-}$, ATDs were also acquired with the quadrupole tuned on $[(T2)_2 + 2NH_4]^{5-}$ (which is present in the mass spectrum in Fig. 2). The ATD for $[(T2)_2 + 2NH_4]^{5-}$ at low injection energy was almost identical to the low injection energy ATD of $(T2)_2^{5-}$ shown in Fig. 4, and a comparable injection energy dependence was observed. The experimental cross sections of $[(T2)_2 + 2NH_4]^{5-}$ were also very similar with the shortest and longest time peaks yielding cross sections of 788 and 840 Å^2. These similarities indicate that the presence of NH_4^+ does not have an effect on the size of $(T2)_2$ (and probably only a small effect on its structure).

Theoretical modeling was utilized to determine the conformation of each peak observed in the ATDs. Multiple strand orientations are possible for a 2-strand quadruplex depending on how the bases between the Gs loop the quartets together. The five different starting geometries modeled are shown in Scheme 2. Parallel (propeller), antiparallel (edge, syn-edge, crossover) and mixed parallel/antiparallel strand orientations were analyzed with no NH_4^+ and $2NH_4^+$ using 300 K dynamics simulations. Only one steady state was observed during the dynamics for each of the different quadruplexes; and similar to the 4-strand complexes, different cross sections were observed for each complex. The theoretical cross sections for $[(T2)_2 + 2NH_4]^{5-}$ were within 1% of the values for $(T2)_2^{5-}$, so Table 2 only illustrates the cross sections for $(T2)_2$ without NH_4^+.

The 300 K dynamics structures for $(T2)_2^{5-}$ and $[(T2)_2 + 2NH_4]^{5-}$ in both an antiparallel and parallel strand orientation are shown in Fig. 5. In all of the different strand orientations for the 2-strand quadruplexes, almost all of the Hoogsteen bonds remain intact. However, the biggest difference between the structures with no NH_4^+ ion and $2NH_4^+$ ions is that the G-quartets are flatter in the structures with $2NH_4^+$, since their carbonyl oxygens are stabilized by the NH_4^+ ion. From the experimental cross sections, the shorter time peak in Fig. 4 (790 Å^2) agrees very well with the cross sections for all of the antiparallel quadruplexes. On the other hand,

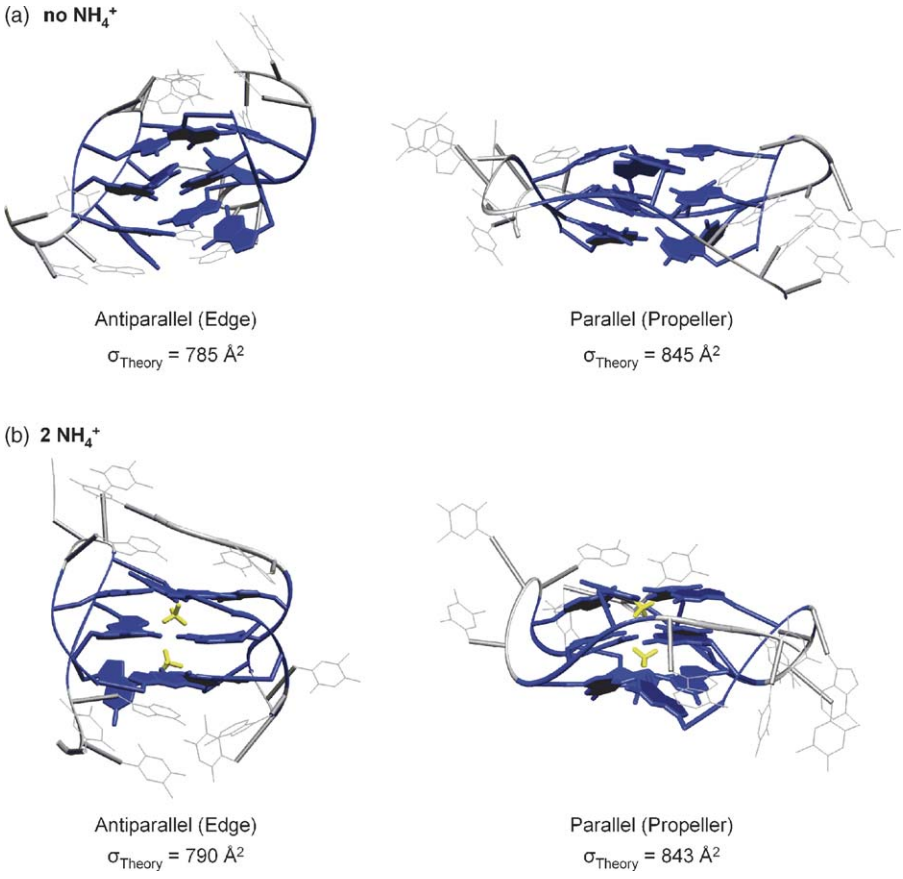

Fig. 5. The theoretical structures for the antiparallel (edge) and parallel (propeller) structures of $(T2)_2$ that match the experimental cross sections (a) without NH_4^+ stabilization and (b) with NH_4^+ stabilization.

Table 2
Experimental and theoretical cross sections (Å^2) of $(T2)_2^{5-}$ [a]

Complex	Cross sections[b]
Experimental	790, 838
Theoretical	
Globular	745
Para: propeller	845
Anti: edge	785
Anti: syn-edge	797
Anti: crossover	788
Para/anti mix	820

[a] Cross sections for $[(T2)_2 + 2NH_4]^{5-}$ were within 1% (data not shown).
[b] 1% reproducibility error for the experimental cross sections and ≤2% S.D. for the theoretical values.

the longer time peak (838 Å^2) only agrees with the parallel propeller quadruplex. From previous ion mobility studies, it has also been found that injection energies from 30 to 40 eV best preserve solution based conformations [44], so the ATD at 30 eV suggests that about 90% of the solution conformers are antiparallel, while only 10% are parallel. The injection energy dependence also indicates that the antiparallel strand orientation is more stable than the parallel conformation, as the latter is no longer present at higher injection energies. These results are similar to the CD results in that two conformers are observed, but ion mobility allows quantification of each strand orientation.

3.3.3. Intramolecular quadruplexes: T4 and T6

The ATDs for all of the observed charge states of T4 and T6 are shown in Fig. 6. All of the ATDs are obtained under similar experimental conditions (injection energy of 30 eV). Single peak ATDs are observed for the −5, −6 and −8 charge states. However, two peaks are present in the −7 charge state for T4 and three peaks for T6. The cross section of each peak was measured and listed in Table 3. It appears that as the charge state becomes more negative, the cross sections increase, probably due to charge repulsion. The ATDs and cross sections for $(T4 + 2NH_4)$ and $(T6 + 2NH_4)$ were also measured and trends similar to the complexes without NH_4^+ were observed.

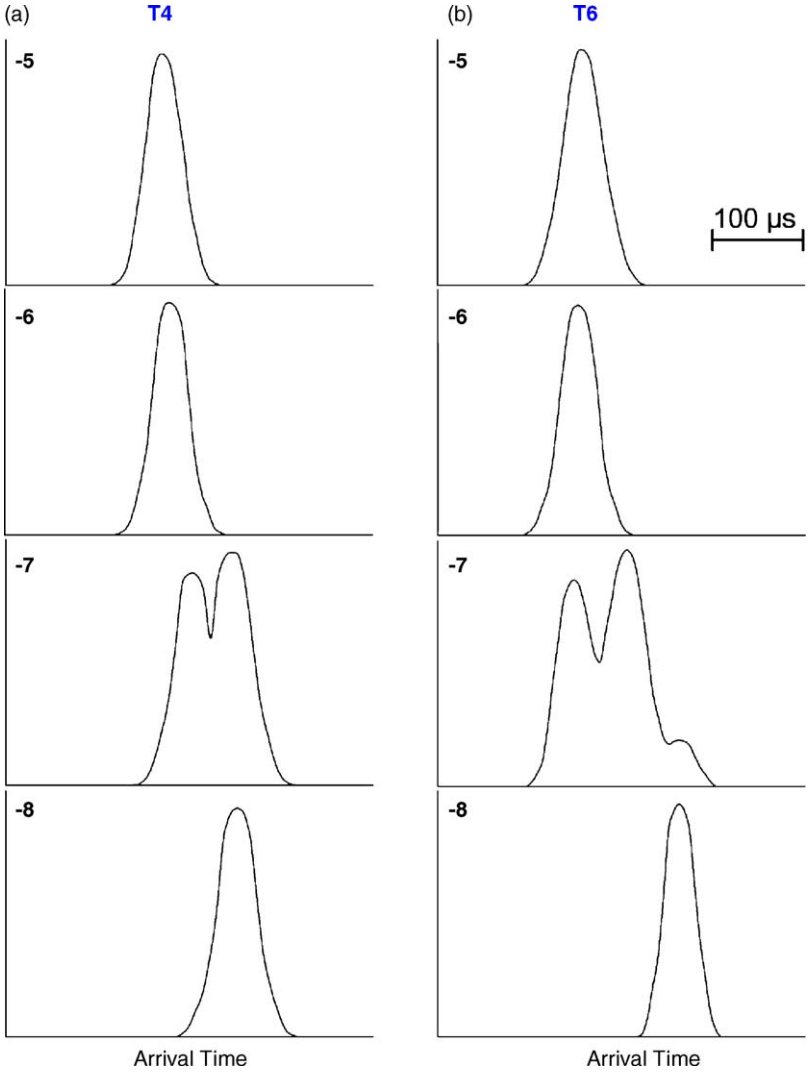

Fig. 6. The ATDs for the different charge states of (a) T4 and (b) T6.

Table 3
Experimental cross sections (Å^2) for T4 and T6 vs. charge state

Complexes	Experimental cross sections[a,b]
$T4^{5-}$	789
$T4^{6-}$	805
$T4^{7-}$	950, 1041
$T4^{8-}$	1054
$T6^{5-}$	989
$T6^{6-}$	1010
$T6^{7-}$	1074, 1232, 1400
$T6^{8-}$	1405

[a] 1% reproducibility error.
[b] T4 and T6 with NH_4^+ adducts had similar cross sections.

Table 4
Theoretical cross sections (Å^2) for $T4^{5-}$[a]

Complex	Theory[b]
Globular	743
Para: propeller	842
Anti: chair	791[c]
Anti: basket	789[c]
Para/anti mix	820

[a] Nearly identical cross sections (and structures) were obtained for $(T4 + 2NH_4)^{5-}$ (data not shown).
[b] ≤2% S.D.
[c] The experimental cross section for $T4^{5-}$ is 789 Å^2.

Theoretical modeling was used to understand why the cross sections become larger with increasing charge state. For T4, several strand orientations are possible for a 1-strand quadruplex (Scheme 2). Parallel (propeller), antiparallel (chair and basket) and mixed parallel/antiparallel strand orientations were analyzed with no NH_4^+ and $2NH_4^+$ using 300 K dynamics simulations. Only one steady state was observed for $T4^{5-}$ in each orientation during the dynamics and the cross sections for $(T4 + 2NH_4)^{5-}$ were within 1% (Table 4).

The structures obtained from 300 K dynamics for $T4^{5-}$ and $(T4 + 2NH_4)^{5-}$ in chair and basket antiparallel strand orientations are shown in Fig. 7. In both of the strand orientations, almost all of the Hoogsteen bonds remain intact, and similar to $(T2)_2$, the biggest difference between the structures with no NH_4^+ ions and $2NH_4^+$ ions is that the G-quartets are flatter in the structures with $2NH_4^+$. When the cross sections of all of the T4 theoretical structures were compared with the single ATD peak for $T4^{5-}$ and $T4^{6-}$, only the antiparallel chair and basket quadruplex structures correlated. In the theoretical calculations for the −7 and −8 charge states of T4, compact quadruplex struc-

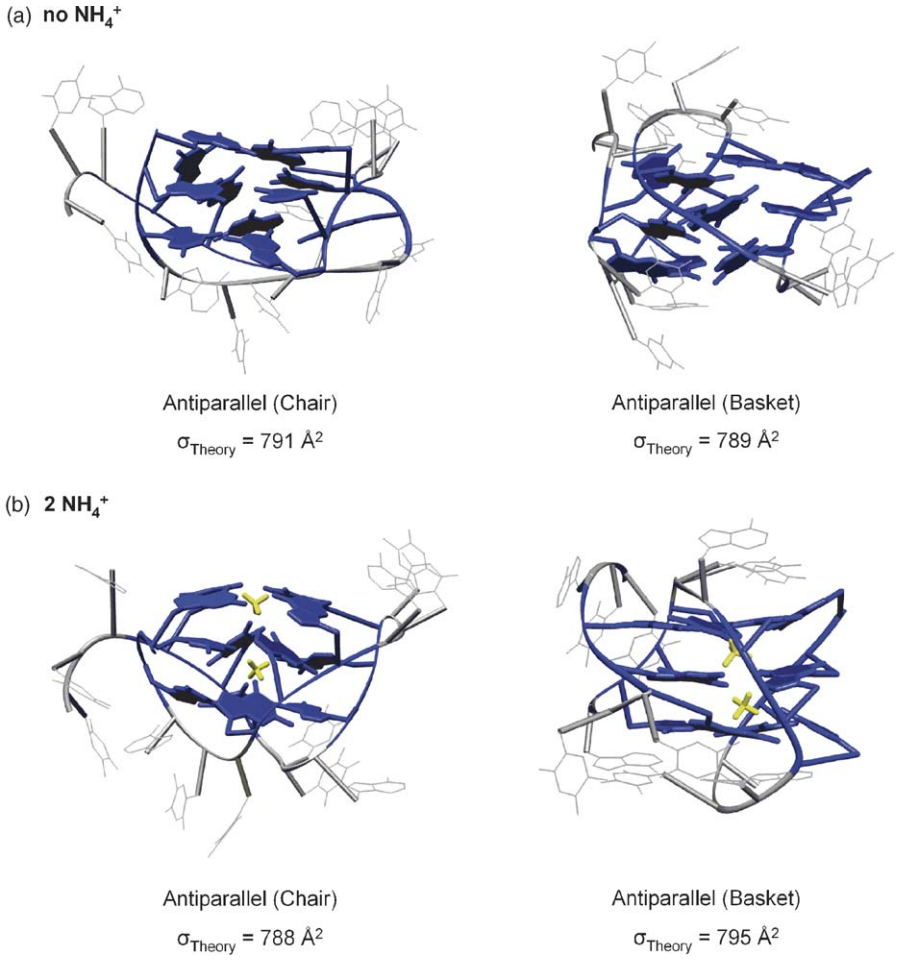

Fig. 7. The theoretical structures for the antiparallel chair and basket structures of $T4^{5-}$ (a) without NH_4^+ and (b) with $2NH_4^+$ that match the experimental cross section of 789 Å^2.

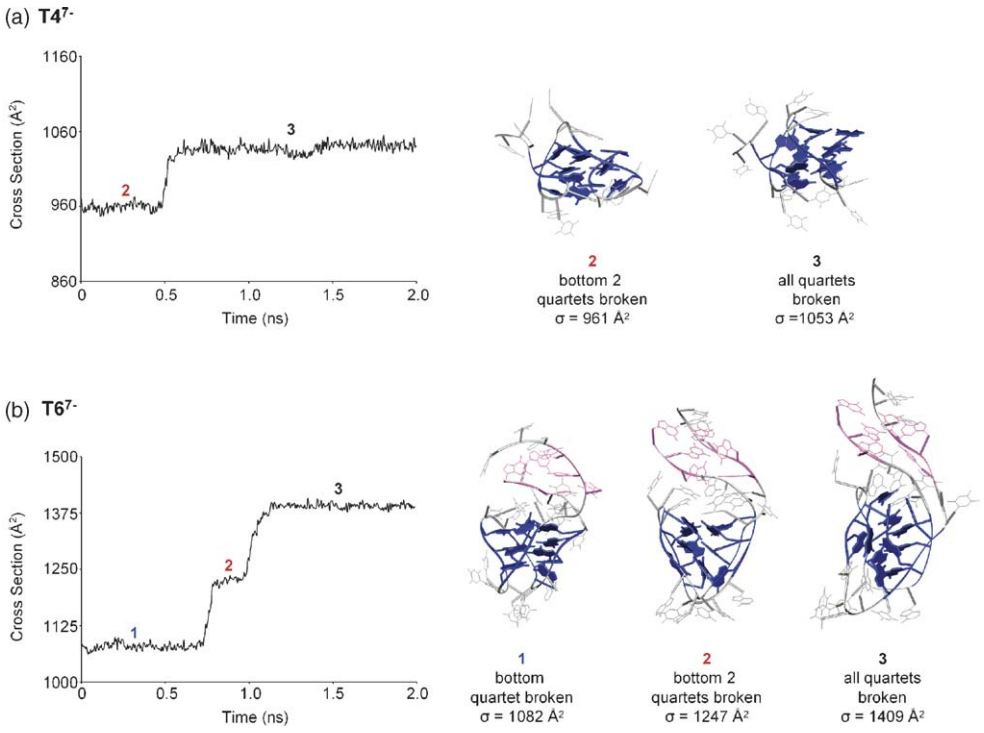

Fig. 8. Plots of cross section vs. time and the resulting stable theoretical structures for (a) $T4^{7-}$ and (b) $T6^{7-}$. Dynamics were run at 300 K for 2 ns and every 5 ps a structure was saved and its cross section calculated. Two steady states were observed in the dynamics for $T4^{7-}$ and three for $T6^{7-}$.

tures like those observed for the −5 and −6 charge states were not present, but instead, the single-strand elongates due to the increased charge repulsion. Two different conformers resulted for the −7 charge state, where two of the G-quartets were broken in the smaller conformer (961 $Å^2$), while all three broke in the larger conformer (1053 $Å^2$). Fig. 8a shows the cross section versus dynamics plot for $T4^{7-}$ and the two resulting structures. Cross sections of these two conformers agreed very well with the two experimental cross sections. Only one conformer at 1064 $Å^2$ was observed for the −8 charge state, and it had a structure similar to the larger conformer of the −7 charge state, in which all of the quartets were broken.

For the T6 starting structures, strand orientations similar to T4 are possible (Scheme 2). However, T6 has two extra G-rich segments that will not be involved in the quadruplexes and their location needs to be determined. Scheme 3 shows that the two extra G-rich repeats can both be at the 5′ or 3′ end, one at the 5′ end and one at the 3′ end, one in a loop and the other at the 5′ or 3′ end, both in separate loops, or both in one loop. The different locations of the two extra G-rich segments were modeled with 300 K dynamics simulations for the propeller, chair, basket and parallel/antiparallel mix structures. The cross sections for $(T6 + 2NH_4)^{5-}$ were within 1% of the values for $T6^{5-}$, so Table 5 only illustrates $T6^{5-}$ cross sections.

When the cross sections of the T6 theoretical structures were compared with the cross sections for $T6^{5-}$ and $T6^{6-}$, only the antiparallel chair and basket quadruplex structures with the two extra G-rich segments on either the 5′ end, 3′ end, or one on each

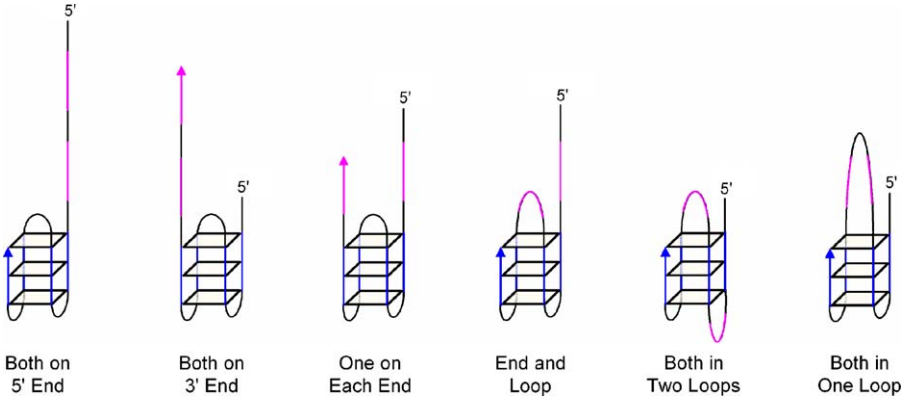

Scheme 3. Different locations for the two extra G-rich repeats of T6 (illustrated on the antiparallel basket conformer). The G-rich segments in the quadruplex are shown in blue and the G-rich segments not in the quadruplex are shown in pink.

Table 5
Theoretical cross sections (Å^2) for $T6^{5-}$ [a]

Complex	Theory[b]				
	Both on 5′ or 3′ end	1 on each end	End and loop	Both in two loops	Both in one loop
Globular	1055	1049	1052	1060	1062
Para: propeller	1083	1092	1120	1141	1159
Anti: basket	1008[c]	1003[c]	1040	1062	1086
Anti: chair	1002[c]	1005[c]	1045	1066	1083
Para/anti mix	1047	1045	1071	1093	1107

[a] Essentially identical cross sections were obtained for $(T6 + 2NH_4)^{5-}$ (data not shown).
[b] ≤2% S.D.
[c] The experimental cross section for $T6^{5-}$ is 989 Å^2.

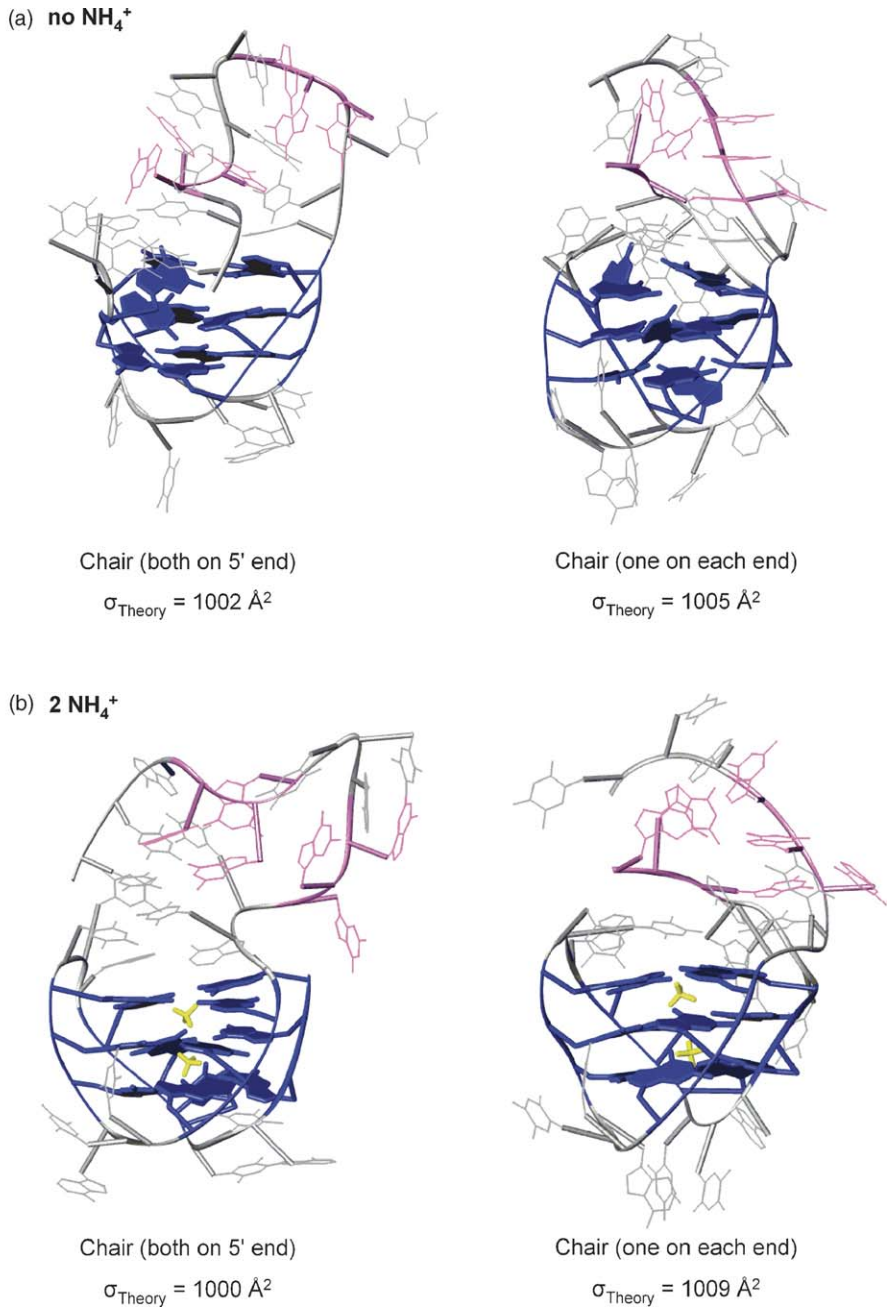

Fig. 9. The theoretical antiparallel chair structures for $T6^{5-}$ in which the two extra T_2AG_3 are either on the 5′ end, or one on the 5′ end and the other on the 3′ end. Structures are shown (a) without NH_4^+ and (b) with $2NH_4^+$.

end (Table 5) were in agreement with the experimental cross section (989 Å^2). The parallel, parallel/antiparallel mix and globular structures were too large to match the experimental cross section, and whenever a G-rich segment was placed in a loop of the antiparallel structures, greater theoretical cross sections were also observed. These results indicate that the −5 and −6 charge states of T6 have an antiparallel structure in which consecutive G-rich regions form the quadruplex. Examples of the steady state 300 K dynamics structures for $T6^{5-}$ and $(T6 + 2NH_4)^{5-}$ in antiparallel chair conformations with the extra G-rich segments on the 5′ end and one on each end are shown in Fig. 9. Almost all of the Hoogsteen bonds remain intact for these strand orientations. These ion mobility results provide a more detailed structural analysis of T6 than the CD results, which were only able to reveal that it had an antiparallel strand orientation.

The theoretical modeling of the −7 and −8 charge states of T6 were similar to T4 as compact quadruplex structures like those observed for the −5 and −6 charge states did not occur. Instead, three different conformers resulted in the −7 charge state where the single-strand elongated due to the increased charge repulsion. The conformers differed in the extent of breakage of these G-quartets as shown in Fig. 8. In the smallest conformer (1082 Å^2), one of the G-quartets broke, two fell apart in the intermediate conformer (1247 Å^2) and all three were broken in the largest conformer (1409 Å^2). The cross sections of these three conformers agreed very well with the three experimental cross sections. Only one conformer at 1416 Å^2 was observed in the −8 charge state, and it had a structure similar to the largest conformer of the −7 charge state where all of the quartets were broken. The cross section of this conformer also agreed within 2% of the experimental cross section.

4. Summary

The mass spectrometry, ion mobility and molecular dynamics results presented in this paper provide several important insights into the solvent-free conformations of dTG_4T, T1, T2, T4 and T6. In particular, we conclude that:

1. dTG_4T and T1 form parallel 4-strand quadruplexes with $2NH_4^+$ adducts for T1 and $3NH_4^+$ adducts for dTG_4T. No 4-strand quadruplexes were observed without NH_4^+ stabilization.
2. T2 forms a 2-strand quadruplex with and without NH_4^+ adducts in which 90% of the conformers have an antiparallel strand orientation, while 10% of the conformers are parallel. The antiparallel strand orientation is also more robust than the parallel conformer, which was easily dissociated at high injection energy.
3. Single-strand antiparallel intramolecular quadruplexes were observed for the −5 and −6 charge states of T4 and T6 with and without NH_4^+ adducts. The two extra T_2AG_3 repeats on T6 are either located both on the 5′ end, 3′ end, or one on each end, indicating that consecutive G-rich segments form the antiparallel quadruplex. As the charge states of T4 and T6 become more negative, broken quartets are observed due to the increased charge repulsion.
4. The solution strand orientations observed in the CD spectra were the same as the solvent-free strand orientations detected in the ion mobility measurements and molecular dynamics calculations strongly supporting structural conservation upon spraying and dehydration of the quadruplexes. Further, the CD measurements could only determine whether the strands were parallel or antiparallel, while the comparison of ion mobility cross sections with model cross sections would often yield much more detailed structural information.
5. In the 2-strand T2 and 1-strand T4 and T6 quadruplexes, the dominant mass spectra peaks resulted from no NH_4^+ stabilization. Hence, these are also the dominant species present in solution since loss of tightly bound NH_4^+ ions during the spray process simply would not occur. This result strongly implies that ionic stabilization of intramolecular G-quadruplexes is not required for the structure to survive.

Acknowledgements

The support of the National Science Foundation under grant CHE-0503728 is gratefully acknowledged. VG is an FNRS (Belgium) Research Associate, and is grateful to the FNRS for funding a research stay at UCSB.

Appendix A. Supplementary data

Supplementary data associated with this article can be found, in the online version, at doi:10.1016/j.ijms.2006.03.016.

References

[1] B. McClintock, Res. Bull. Mo. Agric. Esp. Stn. 290 (1938) 1.
[2] B. McClintock, Genetics 26 (1941) 234.
[3] B. McClintock, Proc. Natl. Acad. Sci. U.S.A. 28 (1942) 458.
[4] H.J. Muller, Collecting Net. 13 (1938) 182.
[5] H.J. Muller, I.H. Herskowitz, Am. Nat. 88 (1954) 177.
[6] E.H. Blackburn, Trends Biochem. Sci. 16 (1991) 378.
[7] E.H. Blackburn, Cell 106 (2001) 661.
[8] S. Haider, G.N. Parkinson, S.J. Neidle, Mol. Biol. 320 (2002) 189.
[9] Y. Wang, D.J. Patel, Structure 2 (1994) 1141.
[10] R. McElligott, R.J. Wellinger, EMBO J. 16 (1997) 3705.
[11] K.E. Huffman, S.D. Levene, V.M. Tesmer, J.W. Shay, W.E. Wright, J. Biol. Chem. 275 (2000) 19719.
[12] W.E. Wright, V.M. Tesmer, K.E. Huffman, S.D. Levene, J.W. Shay, Genes Dev. 11 (1997) 2801.
[13] J. Zhu, H. Wang, J.M. Bishop, E.H. Blackburn, Proc. Natl. Acad. Sci. U.S.A. 96 (1999) 3723.
[14] E.H. Blackburn, Nature 408 (2000) 53.
[15] S. Neidle, M.A. Read, Biopolymers 56 (2001) 195.
[16] E.H. Blackburn, Cell 77 (1994) 621.
[17] D. Sen, W. Gilbert, Nature 334 (1988) 364.
[18] Y. Wang, D.J. Patel, J. Mol. Biol. 234 (1993) 1171.
[19] C. Kang, X. Zhang, R. Ratliff, R. Moyzis, A. Rich, Nature 356 (1992) 126.
[20] F.W. Smith, J. Feigon, Nature 356 (1992) 164.
[21] F.W. Smith, P. Schultze, J. Feigon, Structure 3 (1995) 997.
[22] Y. Wang, D.J. Patel, J. Mol. Biol. 251 (1995) 76.
[23] R. Erlitzki, M. Fry, J. Biol. Chem. 272 (1997) 15881.
[24] G. Fang, T.R. Cech, Cell 74 (1993) 875.
[25] Z. Liu, J.D. Frantz, W. Gilbert, B.-K. Tye, Proc. Natl. Acad. Sci. U.S.A. 90 (1993) 3157.

[26] N. Baran, L. Pucshansky, Y. Marco, S. Benjamin, H. Manor, Nucleic Acids Res. 25 (1997) 297.
[27] H. Sun, J.K. Karrow, I.D. Hickson, N. Maizels, J. Biol. Chem. 273 (1998) 27587.
[28] P. Hazel, J. Huppert, S. Balasubramanian, S. Neidle, J. Am. Chem. Soc. 126 (2004) 16405.
[29] J. Li, J.J. Correia, L. Wang, J.O. Trent, J.B. Chaires, Nucleic Acids Res. 33 (2005) 4649.
[30] A.T. Phan, D.J. Patel, J. Am. Chem. Soc. 125 (2003) 15021.
[31] Y. Wang, D.J. Patel, Structure 1 (1993) 263.
[32] G.N. Parkinson, M.P. Lee, S. Neidle, Nature 417 (2002) 876.
[33] E.M. Rezler, J. Seenisamy, S. Bashyam, M.Y. Kim, E. White, W.D. Wilson, L.H. Hurley, J. Am. Chem. Soc. 127 (2005) 9439.
[34] N. Nagesh, D. Chatterji, J. Biochem. Biophys. Methods 30 (1995) 1.
[35] W. Guschlbauer, J-.F. Chantot, D. Thiele, J. Biomol. Struct. Dyn. 8 (1990) 491.
[36] D. Rovnyak, M. Baldus, G. Wu, N.V. Hud, J. Feigon, R.G. Griffin, J. Am. Chem. Soc. 122 (2000) 11423.
[37] P. Schultze, N.V. Hud, F.W. Smith, J. Feigon, Nucleic Acids Res. 27 (1999) 3018.
[38] R. Giraldo, M. Suzuki, L. Chapman, D. Rhodes, Proc. Natl. Acad. Sci. U.S.A. 91 (1994) 7658.
[39] K. Fukushima, H. Iwahashi, Chem. Commun. 11 (2000) 895.
[40] I. Manet, L. Francini, S. Masiero, S. Pieraccini, G.P. Spada, G. Gottarelli, Helv. Chim. Acta 84 (2001) 2096.
[41] T. Aggerholm, S.C. Nanita, K.J. Koch, R.G. Cooks, J. Mass Spectrom. 38 (2003) 87.
[42] D.R. Goodlett, D.G. Camp II, C.C. Hardin, M. Corregan, R.D. Smith, Biol. Mass Spectrom. 22 (1993) 181.
[43] F. Rosu, V. Gabelica, C. Houssier, P. Colson, E. De Pauw, Rapid Commun. Mass Spectrom. 16 (2002) 1729.
[44] E.S. Baker, S.L. Bernstein, M.T. Bowers, J. Am. Soc. Mass Spectrom. 16 (2005) 989.
[45] W.M. David, J. Brodbelt, S.M. Kerwin, P.W. Thomas, Anal. Chem. 74 (2002) 2029.
[46] M.T. Bowers, P.R. Kemper, G. von Helden, P.A.M. van Koppen, Science 260 (1993) 1446.
[47] G. von Helden, M.-T. Hsu, P.R. Kemper, M.T. Bowers, J. Chem. Phys. 95 (1991) 3835.
[48] T. Wyttenbach, M.T. Bowers, Top. Curr. Chem. 225 (2003) 207.
[49] D.E. Clemmer, M.F. Jarrold, J. Mass Spectrom. 32 (1997) 577.
[50] T. Wyttenbach, P.R. Kemper, M.T. Bowers, Int. J. Mass Spectrom. 212 (2001) 13.
[51] E.A. Mason, E.W. McDaniel, Transport Properties of Ions in Gases, Wiley, New York, 1988.
[52] H.M. Berman, J. Westbrook, Z. Feng, G. Gilliland, T.N. Bhat, H. Weissig, I.N. Shindyalov, P.E. Bourne, Nucleic Acids Res. 28 (2000) 235.
[53] G. Laughlan, A.I. Murchie, D.G. Norman, M.H. Moore, P.C. Moody, D.M. Lilley, B. Luisi, Science 265 (1994) 520.
[54] HyperChem 7.0, Hypercube Inc., 2002.
[55] D.A. Case, et al., AMBER 7, University of California, San Francisco, 2002.
[56] M.F. Mesleh, J.M. Hunter, A.A. Shvartsburg, G.C. Schwartz, M.F. Jarrold, J. Phys. Chem. 100 (1996) 16082.
[57] A.A. Shvartsburg, M.F. Jarrold, Chem. Phys. Lett. 261 (1996) 86.
[58] M. Rueda, S.G. Kalko, F.J. Luque, M. Orozco, J. Am. Chem. Soc. 125 (2003) 8007.
[59] M. Lu, Q. Guo, N.R. Kallenbach, Biochemistry 32 (1993) 598.
[60] J. Gidden, A. Ferzoco, E.S. Baker, M.T. Bowers, J. Am. Chem. Soc. 126 (2004) 15132.